Computer simulations on sputtering mechanisms: Bombardment of single-crystalline Cu(100) by Ar ions

J. Likonen
Technical Research Centre of Finland, Reactor Laboratory, Otakaari 3 A, SF-02150 Espoo, Finland
(Received 22 December 1989)

The sputtering mechanisms of monocrystalline Cu are studied using the binary-collision lattice-simulation code COSIPO. Single-crystal Cu(100) is irradiated with normally incident 5-keV Ar ions. The backward-directed modified recoil flux is compared to the angular distribution of sputtered particles in order to follow the sputtering process. The angular distribution of sputtered particles is directly related to the modified recoil flux and collision cascade anisotropies. Particular attention is given to different mechanisms acting in single-crystalline sputtering. Both the collision sequence and Lehmann-Sigmund mechanisms are found to take place. The collision chains are mainly of the short-range type, except for the ⟨110⟩ replacement and directional ones. The ⟨110⟩ and ⟨100⟩ sequences dominate the angular distribution of sputtered particles. The contribution of defocused sequences is higher than that of replacement and focused ones. The sputtering yield and angular distribution of sputtered particles are evaluated as a function of target thickness. Fifteen atomic layers are sufficient to achieve the bulk yield and spot pattern of sputtered particles that corresponds well to that of a monocrystalline target. The Lehmann-Sigmund model is simulated by employing a target with a varying number of (100) atomic layers on the top of the amorphous bulk. Calculations show that two atomic layers of regular structure on the top of the amorphous bulk reproduces the main features of the spot pattern of sputtered atoms, but is inadequate in explaining the collision sequence mechanisms of monocrystalline sputtering.

I. INTRODUCTION

This paper is the third in the series of collision cascade anisotropy studies in single crystals. The first paper (to be referred to as "I" throughout this paper) concentrated on presenting the method of calculations of the collision cascade anisotropies with particular emphasis on the flux concept.[1] In the second paper (to be referred as "II") we continued the development of the computer code in order to be able to investigate more thoroughly the different mechanisms during collision cascades.[2] In the present paper we concentrate on sputtering mechanisms. The same computational techniques are used here that were described in I and II.

The interest in monocrystal sputtering grew especially after Wehner's discovery[3] that the angular distributions of atoms ejected from single-crystal targets showed maximum intensities in directions corresponding to the more closely packed atomic rows. Silsbee[4] explained the phenomenon by focusing collision sequences as a means for the long-range transport of momentum in crystals at low energies. In addition to Wehner spots, it was observed experimentally that the sputtering yields of monocrystals largely depend on the crystallographic direction of the incident beam.[5,6] This was connected to the varying openness seen in stick-and-ball crystal models when viewed from different directions.[5,7] An alternative to the Silsbee mechanism was developed by Lehmann and Sigmund[8] who proposed a model for preferential sputtering based on collisions of subsurface atoms with surface atoms. They pointed out that the spot pattern could result from the regularity of the surface structure, coupled with random collision cascade in the bulk. This model deals with the reduced length of collision sequences by thermal vibrations of the atoms and with preferential sputtering observed in cases when long-range sequences cannot occur (e.g., for hcp crystals). Furthermore, in early computer simulations it was found that the spot patterns did not necessarily arise as a consequence of focused collision sequences.[9] Neither model turns out to be wholly satisfactory, although both contain elements that must be present in a complete theory of the ejection pattern. In recent computer simulations[10,11] both mechanisms were found to take place in monocrystal sputtering. These mechanisms have been reviewed recently by Robinson[12] and Thompson.[13]

In this paper the purpose is to study various sputtering mechanisms in the case of a monocrystalline target for which theoretical results are crude approximations. If it turns out that the sputtering mechanisms can be well separated from each other, it should be possible to use information from simulations within the theory. A good understanding of the basic mechanisms in cascades and sputtering is thus needed. An analogous idea of dividing the simulation into smaller pieces and of using the results of simulation within theory has already been applied for mixing.[14] Here we merely use recoil flux distributions qualitatively in studying the cascade development and how this leads to sputtering. The comparison and unification to theoretical results will be postponed

to a later occasion.

Recent computer simulations have concentrated either on specific sputtering mechanisms at a time[10,15-17] or in momentum distributions in collision cascades,[18] while the connection between these two phenomena has been totally overlooked. The aim of this paper is to study the contributions of different kinds of collision sequences and Lehmann-Sigmund mechanism in sputtering and compare these results with those in paper II. The Lehmann-Sigmund mechanism is studied more quantitatively than in our recent paper,[19] where stress was laid mainly on qualitative features.

II. THE COMPUTATIONAL MODEL

The COSIPO code is used with the same input parameters as in paper II.[2] A Cu(100) surface is bombarded at normal incidence with 5-keV Ar ions. In brief, the trajectory of each particle is constructed as a series of classical quasielastic binary collisions. All collisions with impact parameters less than $0.72a$ (a is the lattice unit) are evaluated. The Molière potential with screening lengths suggested by Robinson[20] is used to describe the elastic scattering. Inelastic losses are based on the exponential Oen-Robinson model.[21] A target atom is displaced when recoiling with a kinetic energy greater than a threshold value E_d. The recoils in the cascades are followed collision by collision until their energy falls below a threshold energy E_c or they escape the target surface, which is represented by an isotropic or a planar barrier with the sublimation energy as a surface binding energy E_s. In the isotropic barrier model, a particle escapes the surface if its kinetic energy exceeds E_s, whatever its direction may be. In the planar binding model, only the normal component of the velocity of an ejected atom is available to overcome the surface barrier. Consequently, the atom is refracted away from the surface normal. The threshold energies E_d and E_c are chosen to be equal to the sublimation energy. A small binding energy E_b=0.2 eV to the target site is used for atoms diplaced by the projectile. Thermal vibrations with a target temperature 300 K are included by assuming that they are uncorrelated and Gaussian distributed. The collision cascades that are sufficiently dilute and linear take place in a perfect crystal. The modified recoil vector flux $N_r^m(\theta,\phi,z,E)$ and the distribution of sputtered particles are calculated in the way described in I and II. The flux N_r^m includes the contribution of collision sequences transferring only energy in addition to normal mass flow.

Provision is also made for modeling and recording different types of collision sequences in connection with sputtering. They are recorded in a similar way to those previously.[2] In *replacement* chains the projectile replaces the next row atom if the projectile is left with a kinetic energy less than E_c, and it is closer to the target site than to its original lattice site. In *focused* (*defocused*) sequence the knocked-out atom momentum is focused (defocused) from collision to collision. In *directional* chains only the momentum transfer along an atomic row is taken into account. The procedure for the simulation of the Lehmann-Sigmund model was modified slightly compared to the earlier one used in Ref. 19. The target is amorphous with a thin monocrystalline layer at the surface. The amorphous target is a single crystal that is randomly rotated in space after each collision. The number of (100) atomic layers on the top of the amorphous bulk is varied. The neighboring structure is determined by the next collider; i.e., if it turns out that the next collider is beyond the interface, the structure is changed from monocrystal to amorphous or vice versa depending on the direction of the recoil. The next collider is searched from the new structure. The procedure used here somewhat decreases the indefiniteness of the position of the interface compared to the previous one.

III. RESULTS AND DISCUSSION

A. Distributions

In our recent papers we have studied quite thoroughly the effect of target structure[11] and the influence of distinct model parameters[22] (e.g., interaction potential and electronic energy loss) in the sputtering of Cu by 5-keV Ar ions. In papers I and II consideration was given to anisotropies and to several mechanisms acting in collision cascades. The aim of this section is to get a deeper insight into the relation between the angular distribution of the sputtered particles and the cascade anisotropies.

Since about 90% of the sputtering[11] originates from the surface plane, its understanding requires knowledge of the modified recoil flux distribution in the close vicinity of the surface. The backward-directed N_r^m distribution stays practically identical as a function of depth (see paper II). As explained in our paper I, the distribution of sputtered particles can be obtained from the equation $N_s(\theta,\phi) = CN_r^m(\theta,\phi,z=0) \mid \cos\theta \mid$ (C is a constant). The sputtering process can be divided into successive steps. The flux N_r^m through a marker just below the surface is the starting point for the procedure. After passing through this marker the recoil collides with a surface atom. The last collision inside the target does not affect the N_r^m distribution very much because its depth dependence is slight.[2] Once crossing the surface, atoms in the sputtering process undergo surface scattering from some of their close neighbors. The final step is the potential barrier, which the atoms have to overcome. In addition to these, there are collision sequences propagating along the surface. These surface processes also contribute to the sputtering. Thus, the N_r^m distribution just below the surface differs from the angular distribution of sputtered particles in respect of surface processes and potential barrier.

In order to follow the sputtering process, the modified recoil flux distribution near the surface is compared to the angular distribution of sputtered particles in Fig. 1. The combination of elastic and inelastic energy losses used here gives good agreement with experimental results.[22]

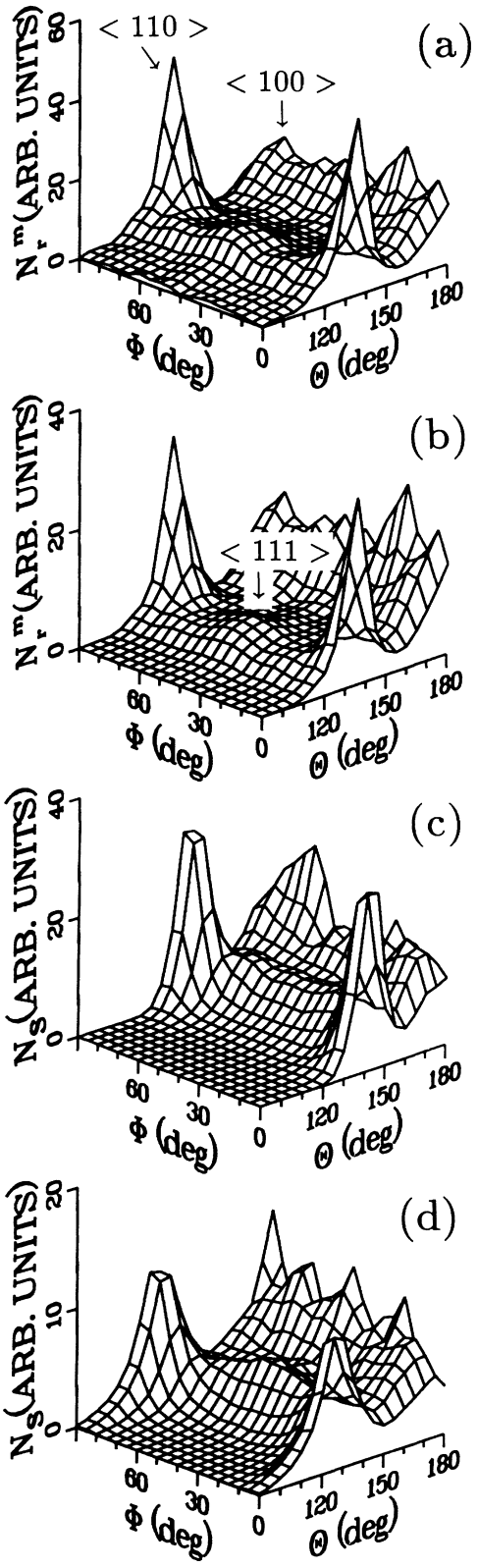

FIG. 1. (a) N_r^m distribution in the backward direction at the depth $z = 0.9$ Å, (b) previous N_r^m distribution multiplied by $\cos\theta$, (c) angular distribution of sputtered particles N_s when isotropic potential barrier is used, and (d) angular distribution of sputtered particles N_s when planar barrier is used.

The experimental distribution of sputtered particles[23] shows four ⟨110⟩ spots and one ⟨100⟩ spot. The intensity of the ⟨100⟩ spot is of the same order as the ⟨110⟩ spots. In Fig. 1(a), the modified recoil vector flux in the backward direction at the depth $z = 0.9$ Å is presented. $\theta = 180°$ corresponds to the backward surface normal and $\theta = 90°$ to direction parallel to the surface. The distribution in Fig. 1(a) has been multiplied by $\cos\theta$ in Fig. 1 (b). The ⟨110⟩ peaks in Fig. 1(b) have become smaller by a factor of $1/\sqrt{2}$ (=| cos 135° |) with respect to the ⟨100⟩ peak.

The recoils in Figs. 1(a) and 1(b) have to undergo collisions when crossing the surface and the surface scattering from some of their close neighbors. Figure 1(c) presents this distribution of sputtered particles in the case of the isotropic potential barrier with E_s equal to the sublimation energy. The isotropic barrier is used only in connection with Fig. 1(c). The planar barrier is employed elsewhere. The spot pattern, when E_s=0 eV, is nearly identical to that in Fig. 1(c). One can observe that the strike between the ⟨110⟩ peaks is shifted towards the surface normal and the small ⟨111⟩ peak has disappeared in Fig. 1(c). In addition to these, the position of the ⟨110⟩ peaks is shifted towards the surface normal, the deflection angle being 5°±3° from the ⟨110⟩ direction. This is in close agreement with MARLOWE results.[10] These changes are due to the surface scattering. In the case of the ⟨111⟩ peak in Fig. 1(a) the effect of the last incomplete focusing ring at the surface is stronger than for the ⟨110⟩ peaks because the angle between the surface normal and the ⟨111⟩ axis is larger and the impact parameter in the last collision smaller than for the ⟨110⟩ row. Thus, the curvature of the band connecting the ⟨110⟩ peaks towards the surface normal is quite logical. The ⟨110⟩ peak heights in Figs. 1(b) and 1(c) are nearly equal. Neglecting the small differences between Figs. 1(b) and 1(c) the distribution of sputtered particles is well related to the modified recoil flux distribution and to the collision cascade anisotropies. In conclusion, the surface scattering is important and does have an influence on the spot pattern. In contrast, surface processes, i.e., collision sequences along the surface, are not important.

The distribution of sputtered particles in the case of the planar surface barrier is shown in Fig. 1(d). The inclusion of the refraction decreases the ⟨110⟩ peaks with respect to the ⟨100⟩ peak and changes the position of the ⟨110⟩ peaks towards the surface by an amount of 5°±3° from the ⟨110⟩ axis. This agrees well with the MARLOWE simulations (9°±2°) (Refs. 10 and 17) and the experimental results (5°±4°) (Ref. 24). In addition to these one can observe preferential ejection in directions parallel to {100} planes intersecting the surface. A comparison with Fig. 1(c) shows that these strikes are due to the refraction of the atom trajectories by the planar binding potential. Calculations show that replacement, focused, and defocused collision sequences contribute to these strikes. Hou and Eckstein[10] have found that only replacement chains provide contributions to these strikes.

The present calculations do not support any pronounced preferential ejection in the ⟨112⟩ direction [see Fig. 1(d)]. Hou and Eckstein have observed ⟨112⟩ spots in the static MARLOWE simulations. Static means that thermal vibrations have been omitted. Experimentally the ⟨112⟩ spots have not been observed, however.[23] On the other hand, the N_r^m distributions have a small ⟨111⟩ peak in Figs. 1(a) and 1(b), which has practically disappeared in Fig. 1(d). Calculations show that the ⟨111⟩ collision sequences are sputtered mainly into a spot with $\theta \approx 43°$ and $\phi \approx 45°$. This position of the spot corresponds to the ⟨112⟩ spot observed by Hou and Eckstein.[10] However, the contribution of all ⟨111⟩ collision chains to this possible ⟨112⟩ spot in the angular distribution of sputtered particles is only little over 1%, and thus the spot is hidden by a background. The fraction of the ⟨112⟩ sequences in this spot is also minor (13%). Overall, the present simulations do not support any preferential ejection in the ⟨112⟩ direction.

B. Contribution of collision sequences to the total yield

In the preceding section it was seen that several directions of predominant sputtering exist. We shall now study the collision sequence mechanisms contributing to the total yield. The fractions of different collision sequences in the sputtering are shown in Fig. 2 as a function of length of the chain. The length $L = 15t_{uvw}$ (t_{uvw} is the unit translation along an axis $[uvw]$) includes all chains with lengths $L \geq 15t_{uvw}$. Table I presents the mean lengths of the ⟨100⟩, ⟨110⟩, and ⟨111⟩ collision sequences and Table II the fractions of the chains contributing to the total yield.

The ⟨110⟩ sequences play the most dominant role in Fig. 2 and the ⟨111⟩ ones the smallest, irrespective of the type of chain. This is due to the fact that the ⟨110⟩ direction has the smallest t_{uvw} and experiences the least energy loss to focusing rings as discussed in paper II. The contributions of long-range ($L \geq 3t_{uvw}$) ⟨110⟩ replacement and directional sequences are also significant. The distributions in Fig. 2 are qualitatively similar to the corresponding ones in paper II (Fig. 6). The sequences are mainly found to be short-range, except for the ⟨110⟩ replacement and directional ones. The sputtering process usually changes the mean lengths of the collision sequences only a little. The mean lengths of the ⟨110⟩ replacement and directional chains have, however, changed about 10%. The higher mean length of ⟨110⟩ replacement sequences in the sputtering is related to the fact that the contribution of long-range ($L \geq 3t_{110}$) chains has increased relatively when Fig. 2(a) is compared to Fig. 6(a) in paper II. The increase of the mean length of ⟨110⟩ replacement and directional chains in the backward direction was also observed in paper II when the depth of the marker decreases. In the case of ⟨110⟩ directional chains, the short-range ($L < 3t_{110}$) sequences have become more dominant, which is partly due to the fact that the mean length of ⟨110⟩ focused chains has decreased. The ⟨110⟩ focused chains have become shorter because long-range ⟨110⟩ chains with low energies cannot overcome the planar surface barrier. For directions other than ⟨110⟩ the mean lengths of the replacement, focused and directional chains have stayed practically constant in most cases. The mean lengths of the defocused sequences

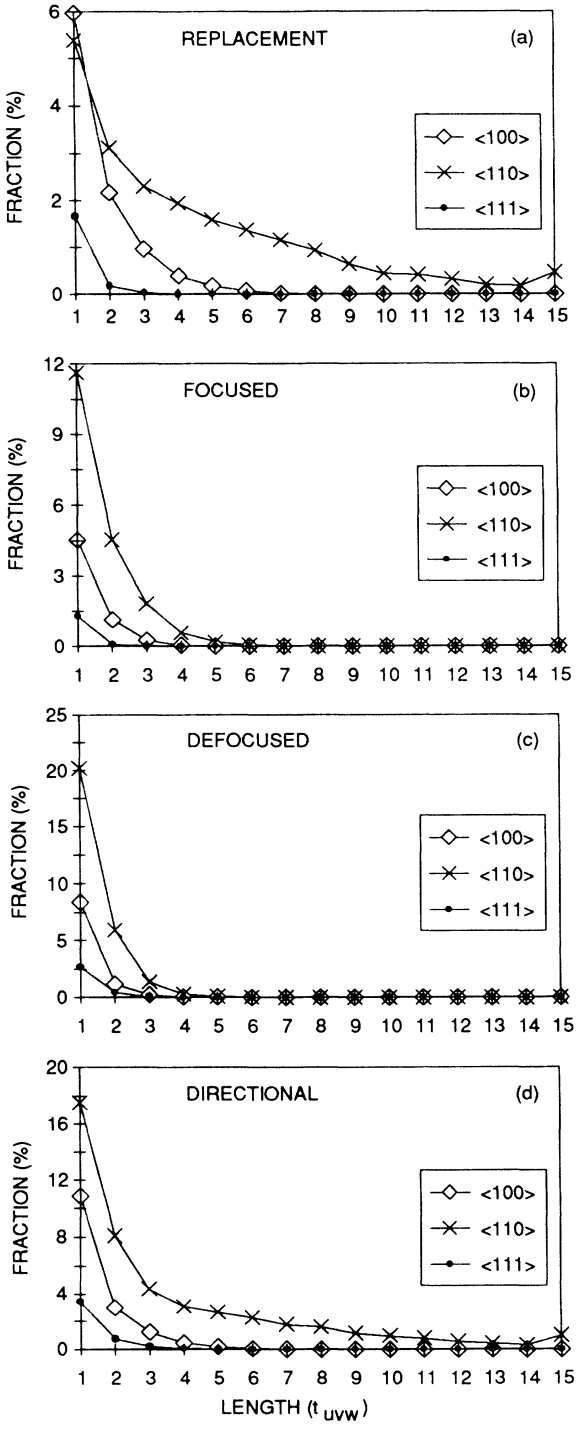

FIG. 2. Contribution of different collision sequences to the sputtering. Replacement sequences are presented in (a), focused in (b), defocused in (c), and directional in (d).

TABLE I. Mean lengths (in units t_{uvw}) of the ⟨100⟩, ⟨110⟩, and ⟨111⟩ collision sequences contributing to the sputtering (S) and the N_r^m distribution (at the depth $z = 0.9$ Å, backward direction). The latter results are from paper II. The statistical uncertainty ΔL is less than $0.05t_{uvw}$ for the ⟨110⟩ replacement and directional chains and for other sequences $0.02t_{uvw}$.

	Replacement		Focused		Defocused		Directional	
Direction	S	N_r^m	S	N_r^m	S	N_r^m	S	N_r^m
⟨100⟩	1.66	1.66	1.31	1.31	1.19	1.23	1.52	1.51
⟨110⟩	4.38	3.93	1.58	1.65	1.36	1.36	3.75	4.13
⟨111⟩	1.14	1.12	1.07	1.08	1.17	1.15	1.36	1.34

have not changed, except in the case of the ⟨100⟩ chains. Most of the ⟨100⟩ chains are perpendicular to the surface and thus are not affected by the refraction of the planar barrier. The ⟨100⟩ defocused chains have become shorter on average. Some comparisons can be made with Shulga's results.[15] The ⟨110⟩ focused chains are shorter and the ⟨110⟩ directional ones longer on average than in Shulga's simulations. The mean lengths of the ⟨110⟩ defocused sequences are equal. The ⟨100⟩ directional chains are shorter than Shulga's result. Reasons for the differences will be discussed in the next section. The different values are understandably due to different model parameters; especially the interatomic potential is stronger in Shulga's work.

All types of ⟨100⟩ chains have become more significant when compared to the contributions to the modified recoil flux at the depth $z = 0.9$ Å in the backward direction (see Table II). This can be attributed to the fact that ⟨100⟩ sequences are more energetic than ⟨110⟩ ones, and thus the effect of the planar surface barrier on the ⟨100⟩ chains is smaller. In the case of the ⟨110⟩ chains, the contribution of the focused sequences has diminished from 25 to 19 % and for other types it has increased. The decrease of the fraction of ⟨110⟩ focused chains is quite natural because the ⟨110⟩ focused chains have mostly low energy, and thus they cannot overcome the planar potential barrier. In addition to this, the ⟨100⟩ and ⟨110⟩ sequences along the surface probably effect the contributions. The role of the ⟨111⟩ chains in the sputtering has not changed as compared to the situation in the modified recoil flux. The contributions of various ⟨111⟩ chains to the modified recoil flux and sputtering are small. The total fractions of various collision sequences in the sputtering have increased except in the case of the focused chains. The changes are mainly due to the fact that the contribution of the main component (⟨110⟩) has changed. Finally, some comparisons can be made with Shulga's results.[15] According to his calculations, the fraction of the ⟨100⟩ directional chains in the total yield is 13%, which is somewhat smaller than our result. Correspondingly, the contributions of the ⟨110⟩ focused, defocused, and directional chains are 30, 23, and 53 %. The role of the focused and directional sequences is somewhat more pronounced than in our calculations, whereas the contribution of the defocused chains in our simulation is higher. Overall, our results are in reasonable agreement with Shulga's.

The contributions of preferential ejection and background in monocrystalline sputtering have been studied experimentally.[25,26] The (100) face of Cu was bombarded with 1–10-keV Cs and Hg ions. The functions describing the preferential ejection in the ⟨110⟩ and ⟨100⟩ directions were Gaussian, whereas the background distribution was represented by a cosine. The contribution of ⟨110⟩ preferential ejection is about 17%, 83% being due to the background.[26] In Ref. 25 the fraction of ⟨110⟩ ejection is 11% and that of the background 89%. In our simulations the preferential ejection in the ⟨100⟩ direction accounts for 5%, the ⟨110⟩ direction 28%, while 67% is due to the background. In both experiments the contribution of ⟨100⟩ ejection was minor or unable to be measured. The differences between the experimental and simulation results can, among other things, be attributed to different ion-target combinations, especially to heavier bombarding ions and denser cascade. As we pointed out, the ratio of the heights of the ⟨110⟩ and ⟨100⟩ peaks is sensitive to interaction potential.[22] In spite of the differences there is a reasonable agreement between the experimental and simulation results.

TABLE II. Contributions (in percentage units) of the ⟨100⟩, ⟨110⟩, and ⟨111⟩ collision sequences to the sputtering (S) and to the N_r^m distribution (at the depth $z = 0.9$ Å, backward direction). The latter results are from paper II. The statistical uncertainty is less than 5%.

	Replacement		Focused		Defocused		Directional	
Direction	S	N_r^m	S	N_r^m	S	N_r^m	S	N_r^m
⟨100⟩	10	7	6	4	10	7	16	12
⟨110⟩	21	16	19	25	28	20	47	45
⟨111⟩	2	2	1	1	3	3	5	4
Total	35	27	27	31	51	38	79	69

C. Contribution of collision sequences to the ⟨100⟩ and ⟨110⟩ spots

The particles are mostly ejected in the ⟨110⟩ and ⟨100⟩ directions with more or less random background. We shall now examine the mechanisms of sputtering into the ⟨100⟩ and the ⟨110⟩ spots. The ⟨110⟩ spot is limited by angles $\theta = 117.5°$–$142.5°$ and $\phi = -12.5°$–$12.5°$, the ⟨100⟩ peak by angles $\theta = 167.5°$–$180°$. Table III presents the contribution of replacement, focused, directional, and all collision sequences to these spots in the sputtering and N_r^m distribution (at the depth $z = 0.9$ Å, backward direction). There are some differences when the results in Table III are compared to each other. In the case of the ⟨110⟩ spots the fractions of directional and all collision chains in the N_r^m distribution and in the sputtering are practically equal. However, the contribution of the replacement and defocused sequences has increased, while that of the focused chains has decreased in the sputtering process. This is due to the fact that the focused sequences have an upper limit for their energy, the focusing energy E_f, which means that chains with energy $E < E_f$ are focused. On the other hand, the replacement sequences have a lower limit $E > E_r$ for their propagation (E_r is replacement energy[27] and $E_r < E_f$). This means that the ⟨110⟩ replacement and defocused sequences are more energetic than the focused ones and thus the effect of the planar surface barrier and the refraction is smaller in the case of the replacement and defocused chains.

In the ⟨100⟩ spot the contribution of directional and all chains has increased in the sputtering process. This is explained by the fact that the fraction of all ⟨110⟩ chains in the ⟨100⟩ spot has increased. The contributions of the replacement and the focused sequences have decreased. This means that the defocused chains have become more significant. The decrease in the contribution of all the focused sequences can be explained by the fact that the fraction of ⟨100⟩ focused chains in the ⟨100⟩ spot is diminished in the sputtering process. Correspondingly, the ⟨100⟩ defocused sequences have become more important because the contribution of the ⟨100⟩ directional ones has not changed in the sputtering process. In the case of replacement chains the decrease in the contribution is connected with the fact that the fraction of ⟨100⟩ replacement sequences in the ⟨100⟩ spot has diminished.

The momentum jump from one atomic row to another is also possible in the case of sputtering. The fraction of all collision sequences in the ⟨100⟩ spot is 79%. The ⟨100⟩ chains contribute 49% and the ⟨110⟩ chains 12%. Correspondingly, in the case of the ⟨110⟩ spots the fraction of all sequences is 90%. The ⟨110⟩ chains have the highest contribution (72%), whereas the ⟨100⟩ chains contribute only 7%. An analogous situation also prevailed in paper II. The fraction of ⟨100⟩ sequences in the ⟨100⟩ spot is equal to the ⟨100⟩ peak in the N_r^m distribution (at the depth $z = 0.9$ Å, backward direction). The contribution of ⟨110⟩ chains to the ⟨100⟩ spot has increased in the sputtering process, which can be attributed to the fact that some ⟨110⟩ defocused sequences are sputtered into the ⟨100⟩ spot. In the case of the ⟨110⟩ spots the increase in the fraction of the ⟨100⟩ sequences and the decrease in the contribution of the ⟨110⟩ chains compared to the N_r^m distribution is due to the fact that the former sequences are more energetic than the latter. Thus, the effect of the planar barrier on the ⟨100⟩ chains is smaller. The ⟨100⟩ sequences, which are sputtered into the ⟨110⟩ spots, are principally defocused, and their contribution increases in the sputtering process. Moreover, some ⟨100⟩ chains along the surface contribute to the ⟨110⟩ spots.

Some comparisons can be made among the results in Table III and other computer simulations. The amount of reference material is quite limited because in other simulations there has been concentration only on specific mechanisms. The differences among the results of various computer codes is due to different model parameters used in the simulations. Thus, exact comparison between distinct codes employed with different model parameters is quite difficult. Shulga[15] bombarded Cu(100) with 27-keV Ar ions (incidence angle 45°), the target temperature being 450 K. The Born-Mayer potential conjugated with power potential was employed. Hou and Eckstein[10] have used a static Cu(100) crystal irradiated with normally incident 5-keV Ar ions and Molière potential. Eckstein and Hou[17] bombarded Au(111) ($T = 15$ K) with 0.6- or 15-keV Xe ions. Yamamura and Takeuchi[16] had the same interaction potential as Hou and Eckstein, though he irradiated the target ($T = 0$ or 300 K) with 1-keV Ar ions. The effect of the thermal vibrations is significant and quite straightforward; they hamper a focused transfer of momentum along an atomic row and result in attenuation of focused collision sequences. The chains get longer when the thermal vibrations are omitted. The changes in the mean lengths are most pronounced for ⟨110⟩ chains; for other directions they are clearly smaller. The total contributions of replacement and focused sequences increase and that of defocused sequences decreases when the thermal vibrations are neglected. The fraction of directional chains does not change. Shulga has made some calculations with normal ion incidence and the results proved to be quite similar to those with the ion incidence angle 45°. The effect of the interaction potential on the collision sequence mechanisms has not been stud-

TABLE III. Contributions (in percentage units) of various collision sequences to the ⟨100⟩ and ⟨110⟩ spots in the sputtering (S) and in the N_r^m distribution (at the depth $z = 0.9$ Å, backward direction). All means the contribution of all types of chains to the ⟨100⟩ and ⟨110⟩ spots. The results for the N_r^m distribution are from paper II. The statistical uncertainty is less than 5%.

	⟨100⟩ peak		⟨110⟩ peak	
Chain	S	N_r^m	S	N_r^m
Replacement	46	54	55	40
Focused	32	36	39	55
Directional	79	71	89	90
All	79	73	90	90

ied systematically, although there are some calculations on the focusing energies based on different interaction potentials,[12] though the overall effect of elastic and inelastic energy losses still requires detailed study. In our previous paper[22] the angular distribution of sputtered particles was found to depend significantly on the interactions between the target atoms. The bombarding energy has a significant effect on the contribution of various collision sequences. These become more significant when the energy increases. According to Shulga[15] the contributions of the directional collision sequences to the ⟨100⟩ and ⟨110⟩ spots are 80 and 90%, which correspond to our results. The fraction of the focused sequences in these spots in our simulations are somewhat lower than in Shulga's calculations (42%). Further comparison with Shulga's results is not possible as Shulga classified the directional collision sequences in a somewhat different way. Moreover, he uses a different definition for the angle between the asymptotes of trajectory and the row axis (see Ref. 15). This changes the results to some degree. In MARLOWE simulations the contributions of the replacement sequences to the ⟨100⟩ spot are 21 and 37% with bombarding energies of 0.6 and 15 keV, respectively.[17] Our result is 46%. In the case of the ⟨110⟩ spots, the fractions of the replacement sequences are 19% (0.6 keV), 46% (5 keV), and 77% (15 keV).[10,17] Also in this case our results are higher. Yamamura and Takeuchi[16] have also made some studies of the contributions of different mechanisms to the sputtering of Cu. According to their simulations, the contribution of the focusing and the assisted focusing to total yield is 37%, which is to some extent higher than our result of 27%. Overall, we may conclude that there is a reasonable agreement between the results of distinct simulations, even though different model parameters have been employed.

D. Dependence on target thickness

The target area and thickness have to be limited in the molecular-dynamics (MD) simulations in practice because the programs are time consuming. This leads to the inability of the lattice of target atoms to contain the entire cascade created by the incident ion, this being called a failure of containment.[28] In this section we study the problem of containment and the contribution of collision processes occurring at the surface. Figure 3 shows the dependence of the sputtering yield on the target thickness. The yield increases quite slowly and reaches a limiting value (bulk yield) for targets thicker than about 15 atomic layers. Thus, to obtain bulk sputtering yield, the target thickness must be sufficient to achieve the bulk incident particle reflection coefficient. The difference between the bulk yield here and in the previous paper[22] is due to the fact that electronic energy loss was omitted in Ref. 22 when calculating the collision kinematics, and due to the larger maximum impact parameter b_{max2} here.

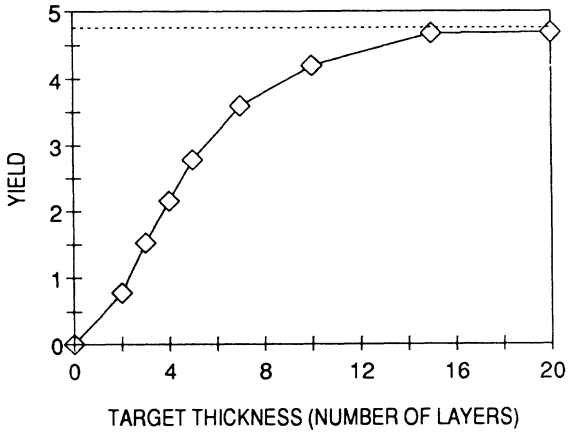

FIG. 3. Dependence of the sputtering yield on the target thickness. The dashed line indicates the bulk yield.

The relation between the angular distribution of sputtered particles and the modified recoil vector flux (in the backward direction at the depth $z = 0.9$ Å) is shown in Fig. 4 as a function of target thickness. In Figs. 4(a) and 4(b), the target contains only two atomic layers. The angular distribution of sputtered particles has two peaks, at $\theta \approx 130°, \phi = 0°, 90°$ [Fig. 4(a)], which correspond to the direction of the ⟨110⟩ spot. The fractions of ⟨100⟩, ⟨110⟩, and all collision sequences in these spots are presented in Table IV. All collision chains make a major contribution to them. The high fraction of ⟨100⟩ sequences in the ⟨110⟩ spots can be attributed, among other things, to the fact that the ⟨110⟩ chains have not been fully developed. In the case of infinite thickness, this contribution is only 7%. In addition to this, some ⟨100⟩ sequences along the surface contribute to the ⟨110⟩ spots in the angular distribution of sputtered particles. The sputtering yield for a target with two layers is about 15% of the bulk

TABLE IV. Contributions (in percentage units) of ⟨100⟩, ⟨110⟩, and all collision sequences to the ⟨100⟩, ⟨110⟩, and ⟨111⟩ peaks in the sputtering (S) and N_r^m distribution (at the depth $z = 0.9$ Å, backward direction). The target thickness is 2 or 4 atomic layers. The statistical uncertainty is less than 10%.

	Two layers			Four layers			
	⟨110⟩	⟨111⟩	⟨100⟩		⟨110⟩		⟨111⟩
Chain	S	N_r^m	S	N_r^m	S	N_r^m	N_r^m
⟨100⟩	24	26	4	2	12	6	16
⟨110⟩	38	21	35	23	42	29	15
All	85	53	54	26	74	46	35

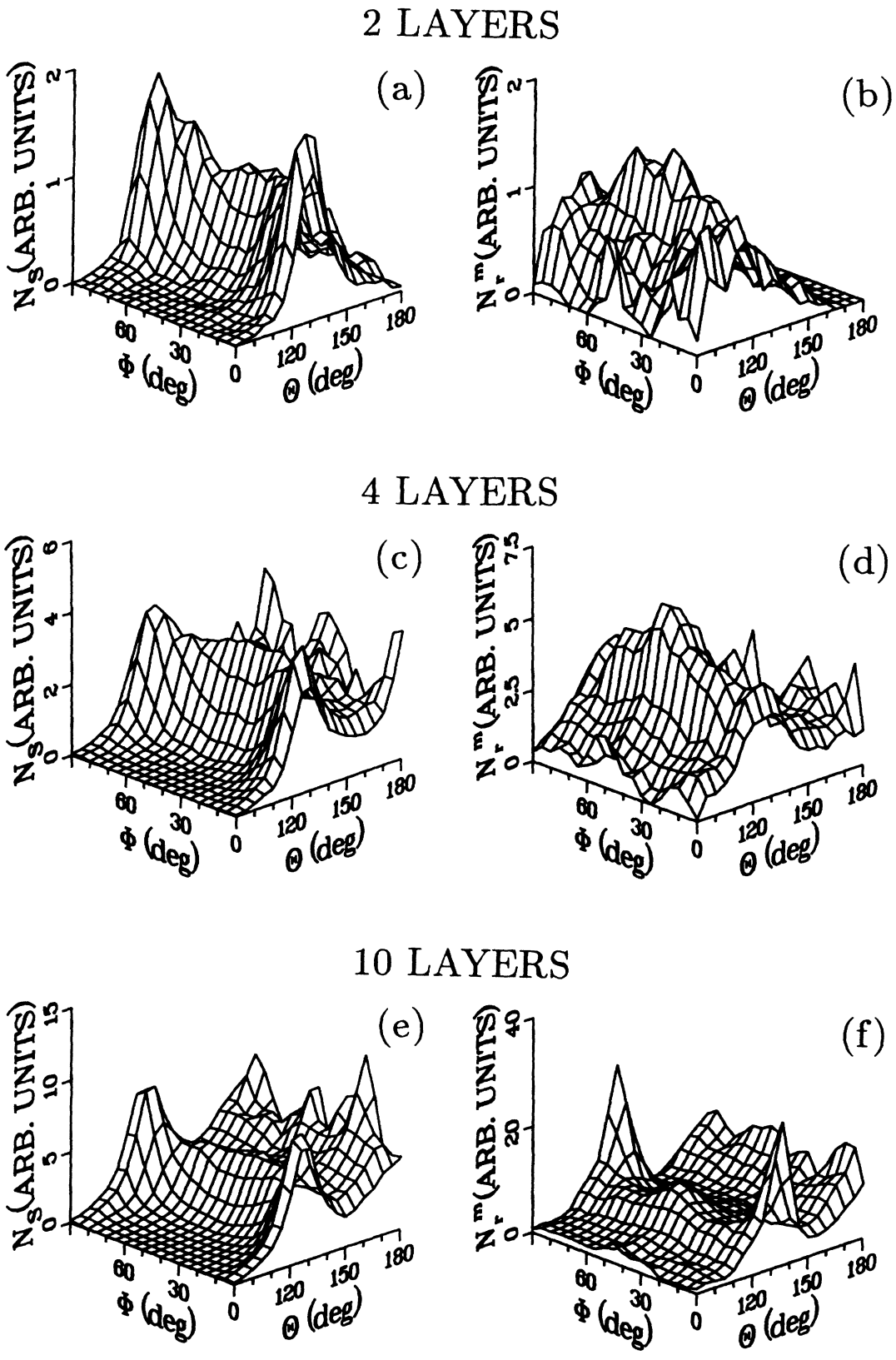

FIG. 4. Spot pattern of sputtered atoms N_s [(a), (c), and (e)] and N_r^m distribution in the backward direction at the depth $z = 0.9$ Å [Figs. (b), (d), and (f)]. The target thickness is 2 for (a) and (b), 4 for (c) and (d), and 10 for (e) and (f) atomic layers.

yield. In addition to this, the number of sputtered atoms in the ⟨110⟩ spots is about 15% of that in the single-crystal case. Thus the collision processes occurring at the surface are not very important in the sputtering of the monocrystalline target. The corresponding N_r^m distribution is totally different [Fig. 4(b)]. It has a peak at $\theta \approx 120°$, $\phi = 45°$. For brevity we will call this direction ⟨111⟩. The fractions of different chains are shown in Table IV. All collision sequences make a major contribution to the ⟨111⟩ peak, though the fractions of ⟨100⟩ and ⟨110⟩ chains are also significant. The recoils moving in the direction $\theta \approx 180^0$ are practically nonexistent, the target thickness being so small that collision sequences cannot be initiated in this direction.

When the target has four atomic layers, the distribution of sputtered atoms [Fig. 4(c)] has two ⟨110⟩ peaks and one ⟨100⟩ peak. The fractions of ⟨100⟩, ⟨110⟩, and all collision chains in these spots are presented in Table IV. The contribution of ⟨110⟩ sequences has increased, and that of ⟨100⟩ chains has decreased in the ⟨110⟩ spots. The role of all collision sequences has also decreased as compared to the two-layer case. All collision sequences make a major contribution to the ⟨100⟩ spot. The fraction of ⟨100⟩ chains is small in this spot. This is due to the fact that the target thickness is so small that ⟨100⟩ chains cannot be created in the direction $\theta \approx 180°$. The contribution of ⟨110⟩ sequences is, however, significant. The N_r^m distribution again is very dissimilar [Fig. 4(d)]. It has a band at $115° < \theta < 130°$ and one ⟨111⟩ peak at $\theta \approx 120°$, $\phi \approx 45°$. The step at $\theta \approx 110°$ is due to the scattering kinematics and was explained in paper II. The fractions of ⟨100⟩, ⟨110⟩, and all collision sequences in the ⟨111⟩ peak have decreased as compared to the case of two layers. Other collision mechanisms have, however, a major role in the ⟨111⟩ peak. The decreased contribution of ⟨100⟩ sequences to the ⟨111⟩ peak can be attributed to the facts that the ⟨100⟩ peak ($\theta = 180°$) has emerged in Fig. 4(d) and the total fraction of ⟨100⟩ collision sequences in the N_r^m distribution has decreased. The ⟨100⟩ peak was not observed in Fig. 4(b). The contributions of different chains to the ⟨100⟩ peak are clearly smaller than in the sputtering. Two small ⟨110⟩ peaks ($\theta \approx 120°$, $\phi = 0, 90°$) start to develop as compared to Fig. 4(b). This explains why the fraction of ⟨110⟩ chains in the ⟨111⟩ peak has decreased. All collision sequences have a major role in the ⟨110⟩ peaks, though the contribution of ⟨110⟩ sequences is also significant. Thus, the increased fraction of ⟨110⟩ chains in the ⟨110⟩ spots in Fig. 4(c) is to be expected. The fact that the spot pattern of sputtered particles and the N_r^m distribution are different from each other shows that the collision processes occurring at the surface are important when the target thickness is small. In the case of single-crystal targets, these surface processes are not, however, very significant.

In Figs. 4(e) and 4(f) the target has ten layers and the distribution of sputtered atoms is qualitatively quite similar to that in Fig. 1(d), where the target thickness is infinite. However, the yield in Fig. 4(e) is 12% smaller than the bulk yield. The contribution of collision chains to the ⟨110⟩ spot (93%) is equal to that in the monocrystalline target, but in the case of the ⟨100⟩ spot the fraction (74%) differs about 5% as compared to the single-crystalline target. The N_r^m distribution [Fig. 4(f)] also is quite similar to that in the case of infinite thickness [Fig. 1(a)]. The ⟨100⟩ and ⟨111⟩ peaks are somewhat more pronounced in Fig. 4(f) than in Fig. 1(a). In the N_r^m distribution the fractions of all collision sequences in the ⟨100⟩ and ⟨110⟩ peaks (64% and 86%) are 13% and 5% smaller than in the case of the monocrystalline target. Figure 4 shows very clearly that a spot pattern of sputtered atoms can be obtained that corresponds quite well to that of the monocrystalline target even though the target thickness is small, i.e., the collision cascade is not fully developed. However, the target thickness must be at least 15 atomic layers in order to achieve the bulk yield and spot pattern that corresponds well to that of the single-crystalline target. In addition to this, the distribution of sputtered particles for a thin target can correspond quite well to the monocrystalline case, though the N_r^m distributions differ markedly from each other. This shows that collision processes occurring at the surface are important when the target is thin but not for a single-crystal target. Thus, the flux-distribution is more sensitive to the thickness than the spot pattern of sputtered atoms. This is due to the fact that there is at least one atomic layer more that the sputtered atoms have to pass after the marker.

Harrison[28] has stated that eight layers are sufficient for absolute containment at 5 keV for the Ar-Cu system. Figure 3 shows that the yield in this case is about 20% smaller than the bulk yield. When the target thickness is ten layers, the yield is 12% lower, but the contributions of all collision sequences to the preferential ejection directions in the sputtering are equal to those for the monocrystalline target. Only when the thickness is 15 layers is the bulk yield achieved. One can conclude that other results reach constant values for thinner targets than those required to produce stable yields. To solve the problem of containment, ten layers seem to be more reasonable than eight in the case of the 5-keV Ar-Cu system. We stress that the containment is not a problem in binary collision approximation (BCA) programs because they are much faster than the MD codes.

E. The Lehmann-Sigmund mechanism

Lehmann and Sigmund[8] have shown that the spot pattern of sputtered particles could result from the random collision cascade in the bulk and the regularity of the surface structure. In this model the predominant ⟨110⟩ sputtering is associated with the surface atoms knocked out by the nearest neighbors in the ⟨110⟩ atomic rows and the predominant ⟨100⟩ sputtering with the second layer atoms that passed through a focusing lens formed by four atoms in the first layer. In the following we study the effect of the number of monolayers on the top of the

TABLE V. The contributions of all collision sequences (in percentage units) to the ⟨100⟩ and ⟨110⟩ peaks in the sputtering (S) and the N_r^m distribution (at the depth $z = 0.9$ Å, backward direction). The target is amorphous with two, four, or ten (100) atomic layers on the top. The statistical uncertainty is less than 5%.

	Two layers		Four layers		Ten layers	
	⟨100⟩	⟨110⟩	⟨100⟩	⟨110⟩	⟨100⟩	⟨110⟩
S	24	76	70	87	78	91
N_r^m	9	13	41	84	74	91

amorphous bulk on the spot pattern of sputtered atoms and flux N_r^m.

Lehmann and Sigmund draw the conclusion that most focused chains must be very short ($1\text{–}2t_{uvw}$) even at high energies of bombarding ions. In the present calculations the fraction of focused and defocused chains with $L > t_{uvw}$ is 20% in the sputtering. If we take into account all focused and defocused sequences of length $L = t_{uvw}$, we can get an estimation for the contribution of the Lehmann-Sigmund mechanism. The fraction of these chains is 59% in the total yield. This is in reasonable agreement with the result of Yamamura and Takeuchi of 64%.[16] However, it must be pointed out that Yamamura and Takeuchi have classified the ejection mechanisms only into three categories, i.e., the Lehmann-Sigmund, the assisted focusing, and the focusing mechanisms. This means that the random background of sputtered particles is included in these mechanisms. Thus, the definitions by Yamamura and Takeuchi of various mechanisms differ somewhat from ours. Therefore the difference between our result and theirs in the case of the contribution of the focused chains is quite natural. In addition to collision sequences, the Lehmann-Sigmund mechanism is also found to have a significant role in single-crystalline sputtering. These two mechanisms may not be totally separated from each other because they both contain collision sequences of length $L = t_{uvw}$. Even if all chains with $L = t_{uvw}$ are assumed to be due to the Lehmann-Sigmund mechanism, the contribution of collision sequences is significant.

The effect of target structure inherent in the Lehmann-Sigmund model on the angular distribution of sputtered particles is shown in Fig. 5 in various situations. The target has two [Figs. 5(a) and 5(b)], four [Figs. 5(c) and 5(d)], or ten [Figs. 5(e) and 5(f)] (100) atomic layers on the top of the amorphous bulk. Thus, the atoms beneath the surface of a regular structure are slowing down randomly. The contributions of different collision sequences are calculated in two ways. In the first case all collision chains are registered, whereas in the second, only focused and defocused sequences of length $L = t_{uvw}$ are included in the distribution. The latter case corresponds better to the Lehmann-Sigmund mechanism, though it is, however, interesting to study also the fractions of all chains. The angular distribution of sputtered atoms [Fig. 5(a)] has two ⟨110⟩ peaks ($\theta \approx 125°$, $\phi = 0, 90°$) and one ⟨100⟩ peak ($\theta = 180°$). The contributions of all collision chains to these spots are presented in Table V and in Table VI those for chains of length $L = t_{uvw}$. The amorphous bulk has decreased the fraction of all sequences in the ⟨110⟩ spot by about 10% (see Table IV). The contribution of focused and defocused chains of length $L = t_{uvw}$ to the total yield is 52%, which is about 10% smaller than in the monocrystalline case. The yield is about 6% higher than the bulk yield. In the case of sequences of length $L = t_{uvw}$ the contribution of these to the ⟨110⟩ spots is practically equal to the fraction of all chains in the ⟨110⟩ spots (see Tables V and VI). Thus, the sequences are mainly of the short-range type. This is due to the fact that the target has only two atomic layers of regular structure. For the ⟨100⟩ spot the difference between the two target structures is significant. The fraction of chains with length $L = t_{uvw}$ in the ⟨100⟩ spot for the target with two layers on the top of the amorphous bulk is only one third of the fraction for the monocrystalline target. This is due to the fact that the ⟨100⟩ focused and defocused chains are undeveloped. Furthermore, it is not straightforward to study the mechanism for the ⟨100⟩ spot in the Lehmann-Sigmund model in the way used here. Thus, the contribution of chains with $L = t_{uvw}$ to the ⟨100⟩ spot does not quite correspond to the situation in the Lehmann-Sigmund model. The N_r^m distribution [Fig. 5(b)] has more pronounced ⟨100⟩ and ⟨110⟩ peaks than in Fig. 5(a). The N_r^m distribution deviates markedly from that in Fig. 4(b). The peak at $\theta \approx 120°$ has practically disappeared and the dominant ⟨100⟩ and ⟨110⟩ peaks have emerged. The contribution of all collision sequences to these peaks is minor because there is only one atomic layer of regular structure below the marker. When the contributions of all collision sequences to the ⟨100⟩ and ⟨110⟩ spots in the angular distribution of sputtered particles (Table V) are compared to the fractions in Table III one can observe that the

TABLE VI. Contributions (in percentage units) of focused and defocused sequences of length $L = t_{uvw}$ to the ⟨100⟩ and ⟨110⟩ spots in the sputtering. The target has two or four (100) atomic layers on the top of the amorphous bulk. Mono stands for monocrystalline target. The statistical uncertainty is less than 5%.

Layers	⟨100⟩ peak	⟨110⟩ peak
2	21	73
4	66	62
Mono	60	62

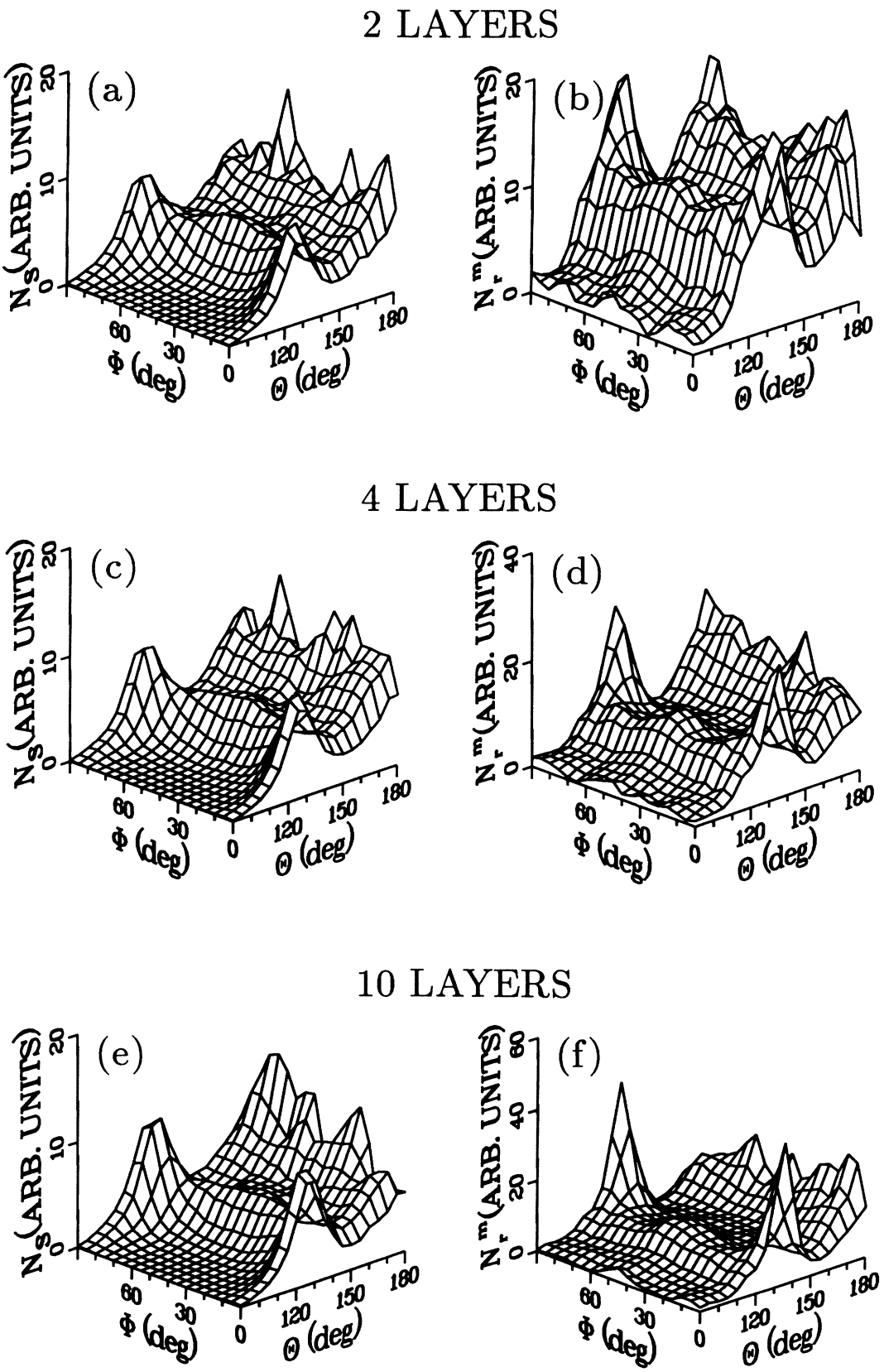

FIG. 5. Angular distribution of sputtered atoms N_s [(a), (c), and (e)] and N_r^m distribution in the backward direction at the depth $z = 0.9$ Å [(b), (d), and (f)]. The target has 2 for (a) and (b), 4 for (c) and (d), and 10 for (e) and (f) (100) atomic layers on the top of the amorphous bulk.

former results are 70% ($\langle 100 \rangle$) and 15% ($\langle 110 \rangle$) smaller than the latter ones. For the N_r^m distribution (in the backward direction, at the depth $z = 0.9$ Å) the differences are even more dramatic. Finally, one can conclude that the Lehmann-Sigmund model with two (100) atomic layers on the top of the amorphous bulk proves to be inadequate in explaining the collision sequence mechanisms of monocrystalline sputtering. In addition to this, the model reproduces the main features of the spot pattern of sputtered atoms.

In the case of four (100) layers the angular distribution of sputtered particles [Fig. 5(c)] is qualitatively similar to that in Fig. 4(c), where the target thickness is four atomic planes. The amorphous bulk has a significant effect on the contribution of all collision sequences to the $\langle 100 \rangle$ and $\langle 110 \rangle$ spots when Tables IV and V are compared with each other. The amorphous bulk increases the fraction of all collision chains by about 30% in the $\langle 100 \rangle$ spot and 20% in the $\langle 110 \rangle$. When the contributions in Table V are compared with those in Table III, one can observe that the results are still smaller than for the totally monocrystalline target, the differences being about 10% in the sputtering. The contributions of focused and defocused sequences of length $L = t_{uvw}$ to the $\langle 110 \rangle$ spots are equal for monocrystalline and amorphous targets with four (100) layers on the top (see Table VI). For the $\langle 100 \rangle$ spot the contributions differ by about 10%. In the case of the monocrystalline target the major contribution of focused and defocused chains of length $L = t_{uvw}$ to the $\langle 100 \rangle$ and $\langle 110 \rangle$ spots in the sputtering is significant. The fraction of the Lehmann-Sigmund mechanism in the total yield is practically equal to that in the monocrystalline case. The yield is about 6% higher than the bulk yield. The N_r^m distribution [Fig. 5(d)] has pronounced $\langle 100 \rangle$ and $\langle 110 \rangle$ peaks. In addition to these, there is also a small $\langle 111 \rangle$ peak. The $\langle 100 \rangle$ peak is more dominant than in Fig. 4(d). The fractions of all collision sequences in the $\langle 100 \rangle$ and $\langle 110 \rangle$ peaks are clearly smaller than the corresponding ones in Table III. In fact, the Lehmann-Sigmund model with four atomic layers would explain the sputtering mechanisms better than the two-layer model. There are still, however, some minor differences as compared to the totally monocrystalline target. Harrison *et al.*[9] and Hou and Eckstein[10] have come to the conclusion that the Lehmann-Sigmund model has to be extended up to the fourth layer from the surface. They used, however, arguments quite different from ours. It must be pointed out that four (100) atomic layers on the top of the amorphous bulk are entirely inadequate for studying the relation between the angular distribution of sputtered particles and vector fluxes.

In Figs. 5(e) and 5(f), the target has ten (100) atomic layers on the top of the amorphous bulk. The angular distribution of sputtered particles and the N_r^m distribution are similar to those in Figs. 4(e), 4(f), and 1. The sputtering yield in this case is equal to the bulk yield. The fractions of collision sequences in the $\langle 100 \rangle$ and $\langle 110 \rangle$ spots in sputtering (see Table V) are equal to those in Table III. The amorphous bulk has practically no effect on the contribution of collision chains to the $\langle 110 \rangle$ spot in the sputtering, though in the N_r^m distribution the bulk increases the fraction by about 5%. In the case of the $\langle 100 \rangle$ spot the amorphous bulk increases the contribution of sequences by about 5% in the sputtering and 15% in the N_r^m distribution. The fractions of all collision chains in the $\langle 100 \rangle$ and $\langle 110 \rangle$ peaks in the N_r^m distribution are practically equal to those in Table III. Moreover, the Lehmann-Sigmund mechanism is found to have a similar role to that in the case of the monocrystalline target. The mean lengths of the $\langle 110 \rangle$ replacement and directional collision chains in the sputtering are almost 20% less than for the monocrystalline target. For other chains the mean lengths are equal to those for the monocrystalline target. Thus, the distributions for the target with ten (100) atomic layers above the amorphous bulk correspond well to the N_r^m distribution (near the surface) and spot pattern of sputtered particles of the monocrystalline target. However, when compared to the target with a thickness of ten atomic layers, the bulk has a clear effect on the N_r^m distribution. These calculations show that even though the contributions in the case of ten (100) atomic layers on the top of the amorphous bulk are equal to those for the monocrystalline target, the mean lengths do not necessarily coincide.

IV. CONCLUSIONS

This paper completes the study of collision cascade anisotropies and monocrystalline sputtering, which was started and continued in papers I and II. The use of marker planes has shown their usefulness in exploring the evolution of collision cascade anisotropies, the relation between the recoil vector fluxes and the distribution of sputtered particles as well as the collision sequence mechanisms in the cascade and sputtering.

In the case of the sputtering of a (100) surface, the distribution of sputtered particles shows four $\langle 110 \rangle$ spots and one $\langle 100 \rangle$ spot. The combination of the interaction potential and electronic energy loss used in this paper gives good agreement with experimental and other computer simulation results. No preferential ejection in the $\langle 112 \rangle$ direction was observed. The linear collision chains are the principal mechanisms in the angular distribution of sputtered particles. Replacement and defocused sequences make a major, and focused chains a smaller, contribution to the total yield. Chains along the $\langle 110 \rangle$ directions are most frequent, with the $\langle 111 \rangle$ sequences making the least contribution. The collision chains are mainly of the short-range type except for the $\langle 110 \rangle$ replacement and directional ones. The momentum can jump from one atomic row to another and the $\langle 110 \rangle$ sequences contribute to the $\langle 100 \rangle$ spot, and the $\langle 100 \rangle$ chains to the $\langle 110 \rangle$ spots.

The sputtering yield and angular distribution of sputtered particles were studied as a function of target thickness. The yield is strongly dependent on the thickness and increases when the target becomes thicker. To ob-

tain the limiting value for the yield the thickness must be sufficient (at least 15 atomic layers in the case studied). The spot pattern of sputtered particles can correspond quite well to that of the monocrystalline target although the thickness is small. However, the backward-directed N_r^m distribution near the surface is totally different from the spot pattern of sputtered atoms in the case of thin targets. The failure of containment, which is associated with thin targets, may become a problem in molecular-dynamics simulations if special caution is not exercised. In addition to collision sequences, the Lehmann-Sigmund mechanism is found to take place in the sputtering of single-crystalline Cu by Ar ions. However, the Lehmann-Sigmund model with two (100) atomic layers on the top of the amorphous bulk is not sufficient to explain the collision sequence mechanisms in monocrystalline sputtering. The model reproduces the main features of the spot pattern of sputtered atoms. Four atomic layers of regular structure on the top of the amorphous bulk would give better correspondence with the monocrystalline sputtering. However, when the relation between the angular distribution of sputtered particles and vector fluxes is studied, four (100) atomic layers on the top of the amorphous bulk is inadequate.

The contributions of various collision sequence mechanisms were compared to experimental and other computer simulation results. Even though different ion-target combinations and model parameters were employed, the results turned out to be in a reasonable agreement.

ACKNOWLEDGMENTS

It is a great pleasure to thank Dr. M. Hautala for his many inspiring comments on the simulations and on the manuscript.

[1] M. Hautala and J. Likonen, Phys. Rev. B **41**, 1759 (1990).
[2] J. Likonen and M. Hautala, Phys. Rev. B **42**, 3838 (1990), preceding paper.
[3] G. K. Wehner, J. Appl. Phys. **26**, 1056 (1955); Phys. Rev. **102**, 690 (1956).
[4] R.H. Silsbee, J. Appl. Phys. **28**, 1246 (1957).
[5] P.K. Rol, J.M. Fluit, F.P. Viehbock, and M. de Jong, in *Proceedings of the 4th International Conference on Ionization Phenomena in Gases, Uppsala, 1959*, edited by N.R. Nilsson (North-Holland, Amsterdam, 1960), pp. 257–259.
[6] G. Almén and G. Bruce, Nucl. Instrum. Methods **11**, 257 (1961).
[7] P.K. Rol, J.M. Fluit, and J. Kistemaker, Physica **26**, 1009 (1960).
[8] C. Lehmann and P. Sigmund, Phys. Status Solidi **16**, 507 (1966).
[9] D.E. Harrison, Jr., J.P. Johnson III, and N.S. Levy, Appl. Phys. Lett. **8**, 33 (1966).
[10] M. Hou and W. Eckstein, Nucl. Instrum. Methods B **13**, 324 (1986).
[11] J. Likonen and M. Hautala, Appl. Phys. A **45**, 137 (1988).
[12] M.T. Robinson, in *Sputtering by Particle Bombardment I*, edited by R. Behrisch (Springer-Verlag, Berlin, 1981), pp.73–144.
[13] M.W. Thompson, Phys. Rep. **69**, 335 (1981).
[14] M. Hautala and I. Koponen, Nucl. Instrum. Methods B **48**, 504 (1990).
[15] V.I. Shulga, Radiat. Effects **70**, 65 (1983); **82**, 169 (1984); **84**, 1 (1985).
[16] Y. Yamamura and W. Takeuchi, Nucl. Instrum. Methods B **29**, 461 (1987).
[17] W. Eckstein and M. Hou, Nucl. Instrum. Methods B **31**, 386 (1988).
[18] M. Hou and W. Eckstein, Max-Planck-Institut für Plasmaphysik, Report No. IPP 9/65, 1988 (unpublished).
[19] M. Hautala and J. Likonen, Nucl. Instrum. Methods B **33**, 526 (1988).
[20] M.T. Robinson and I.M. Torrens, Phys. Rev. B **9**, 5008 (1974).
[21] O.S. Oen and M.T. Robinson, Nucl. Instrum. Methods **132**, 647 (1976).
[22] J. Likonen and M. Hautala, J. Phys. Condens. Matter **1**, 4697 (1989).
[23] A.L. Southern, W.R. Willis, and M.T. Robinson, J. Appl. Phys. **34**, 153 (1963).
[24] C. H. Weijsenfeld, Ph.D. thesis, Utrecht, 1966; Philips Research Reports Supplements, No. 2, 1967 (unpublished).
[25] N.T. Olson and H.P Smith, Jr., Phys. Rev. **157**, 241 (1967).
[26] R.G. Musket and H.P. Smith, Jr., J. Appl. Phys. **39**, 3579 (1968).
[27] M.W. Thompson, in *The Interaction of Radiation with Solids*, edited by R. Strumane, J. Nihoul, R. Gevers, and S. Amelinckx (North-Holland, Amsterdam, 1964), pp. 84–113.
[28] D.E. Harrison, Jr., Radiat. Effects **70**, 1 (1983).